Robotics and Autonomous Systems 102 (2018) 1–12

Contents lists available at ScienceDirect

Robotics and Autonomous Systems

journal homepage: www.elsevier.com/locate/robot

A metric to design spring stiffness of underactuated fingers for stable grasp

Jing Cui [a], Shaobo Yan [b], Jian Hu [b], ZhongYi Chu [b,*]

[a] School of Mechanical Engineering and Applied Electronics, Beijing University of Technology, Beijing, China
[b] School of Instrument Science and Opto-electronics, Beihang University, Beijing, China

HIGHLIGHTS

- We propose a metric for the design of underactuated fingers.
- We get the spring stiffness's delimiter between regimes and the bifurcations of different grasp topology.
- We explore the possibility of using the spring as a design parameter.

ARTICLE INFO

Article history:
Received 2 January 2017
Received in revised form 17 December 2017
Accepted 2 January 2018

Keywords:
Underactuated fingers
The delimiter of spring stiffness
Grasp stabilization
Adaptation of grasping

ABSTRACT

The underactuated hand has the advantage of adaptation for grasping irregularly shaped objects by combining the active actuators with passive springs to achieving a stable grasp. The design of the spring parameter will affect the region of the stable grasp. This paper presents a metric to design the spring stiffness to keep the tradeoff between the adaption of objects and ability of stable grasp. Firstly, the relationship between the spring stiffness and stable region is qualified and visualized according to grasp-state plane together with the spring stiffness's delimiter between regimes. Then, a quantitative way by analytical equations and graphs is proposed to evaluate the grasp stabilization with respect to spring stiffness. Finally, applications of designing the optimal spring stiffness by giving the particular conditions are presented to validate the efficiency of the proposed method.

1. Introduction

On-orbit services using mechanical arm, such as assembling the space station, repairing or retrieving the satellite, refueling the spacecraft are essential for extravehicular activities. As a critical part of the mechanical arm system, the behavior of the end effector could decide on-orbit services level to some extent. In the past few years, various types of end effectors have been studied. A special emphasis has been placed on underactuated robotic hands, in which the degrees of freedom (DOF) is more than the number of actuators and generally uses passive elements in their unactuated joints [1]. In an underactuated finger, the action of an active motor on the phalanges is transmitted through suitable mechanical instruments, e.g. tendon-actuated mechanisms and linkage-based mechanisms, etc [2]. Pioneer designs the MARS and the SARAH hands [3] which have the ability to conform to various unknown objects of large size. The MARS hand was the first underactuated hand which is built to study grasping strategies, each finger can be controlled independently to obtain different grasp types by mounting on top of actuated module. In order to further reduce actuators' amount and as a result decrease the required complexity of controller, SARAH hand is built based on the coupling between different fingers [3]. The SDM hand [4] has the same application with the SARAH hand, while Odhner focused on designing an underactuated finger to pick up small objects from a flat surface [5]. As for an underactuated hand, its compliance is not strictly necessary to conform to various objects; moreover, the null space inherent in underactuation also plays an important role. Applications in the literature show that the underactuated hands have the superiorities of cost, weight and controllability compared with the fully actuated hands [6–8], and can grasp various objects in diverse tasks as the fingers have the ability of adapting to the various object by their inherent mechanical property [9]. This means that the underactuated hands are suitable for implementing the operations of picking up and placing task for different objects under unstructured environments.

Due to the underactuated character, many different types of passive elements were considered [3] to resolve the non-uniqueness question involved with the null space grasp [10], when

* Corresponding author.
E-mail addresses: cuijing@bjut.edu.cn (J. Cui), yanshaobo@sisoe.buaa.edu.cn (S. Yan).

https://doi.org/10.1016/j.robot.2018.01.001
0921-8890/

the finger is not in contacting with an object. Therefore, the problem of grasp stability is the crux of designing an underactuated hand. Generally, form-closure was used to characterize the grasp's robustness. Krut focused on it and extended this property by adding a one-way movement mechanism to implement static constraint between phalanges and the object [11]. However, this method is with the assumption that the contact points between finger and object are fixed in space. When a grasp is exerted by an underactuated hand, it is impossible to control each phalanx's position independently. Although underactuated fingers have a distinct advantage of grasping various objects, there are only a few available tools to solve the grasp stability problem numerically, and the underactuated fingers are designed intuitively. Among a wide range of underactuated hands in research, adaptability and stabilization are usually considered to evaluate the effect of grasping, and improving the level of stabilization is especially important for on-orbit services.

To achieve a stable operation, a novel design of an adaptive neuro fuzzy inference strategy (ANFIS) for controlling input displacement of a new adaptive compliant gripper is presented [12]. Dalibor and Danesh presented a adaptive control algorithm using extreme learning machine (ELM) and support vector regression (SVR) [13]. Kragten, Herder and Gosselin did systematic work. With underactuated fingers able to conform to the object in a stable and multipoint way, they presented a visualized method which called grasp-state plane to attain the stable and ejection regions. Combining this method with the isotropy of a grasp, they proposed a rule to design the underactuated finger [3]. And also there are some classical theory can be used to design the underactuated finger, like TRIZ [14]. To solve the grasp stability problem numerically and produce analytical expressions, Kragten and Herder presented a method in [9]. They focused on bifurcations between grasps of different topology to determine the geometrics' dimensions and actuators' parameters of an underactuated hand so that it could grasp the objects in desired range, since individual joint angles cannot be set by the actuators in underactuated hands, the contact point can move. In addition, the effect of the number of contact points and even contact forces on the stable grasp was pointed out in [15]. For enveloping, the greater number of these contact points and forces with uniformity distribution, the better the grasp capability is. Ciocarlie presented a quasi-static equilibrium formulation to produce the underactuated hand for various grasping tasks [16] and to predict a given grasp's stability [17]. [18] presented one passive compliant joint which have soft contacts with external objects and measurement capabilities. And conductive silicone rubber was used as material for modeling of the compliant segments of the robotic joint. Giannaccini presented a lower cost, cable driven gripper and showed how its compliance can be varied passively to ensure an adaptive yet stable grasp [19]. However, the spring was often neglected in the process of mathematical modeling, or although it has been used in design of the hand but the particulars of the spring, such as its stiffness, were not critical. Under this situation, the spring was usually regarded as a "weak spring", which only used restraint the finger kinematically and ensure the adaptation for the shape of the grasped object, while true spring can make the various grasp types transitioning from one to another with varying the contact forces.

For the underactuated fingers, the appropriate application of the spring makes it possible for one input torque to drive a finger that has more than one DOF [11,20]. The balance between the contact forces, the motor actuation torque and the spring passive torque contributes to various grasp type makes great effect on the stable grasp. If the stiffness of springs is designed too small, underactuated fingers can adapt the shape of objects easily but have less stabilization; If the stiffness of springs is designed too hard, the grasp becomes more stable but could not adjust itself to a widely range of irregularly shaped object. That is to say, an opening ejection or a closing ejection can occur when stiffness is greater or smaller beyond a limitation, and it will lead to a fail mission [9]. To overcome this lack of interrelated knowledge, the purpose of this paper is to propose a metric that is useful in the design of underactuated fingers of the type driven by links. The innovation of the work here is to explore the possibility of designing the spring stiffness to keep the trade-off between the ability of conforming to the object and the stability of grasping. Firstly, an underactuated finger and the corresponding stable region are deducted through statics analysis. As a 5-bar link with only one input torque is indeterminate, a spring which is in a different location from that of the SARAH hand is used to resolve the indeterminacy so that distal phalanges can move relative to one another in the parallel manner with less energy consumption. Then, the paper takes the result of Kragten and Herder on grasp stability and bifurcations in the grasp type to obtain the spring stiffness's delimiter between regimes. Finally, the relationship between spring stiffness and stable region can be visualized in order to obtain the proper spring.

The paper is organized as following. In Section 2, the statics analysis of the underactuated fingers and the stable region in the grasp-state plane are reviewed. In Section 3, the range of spring stiffness is figured out to be regarded as a delimiter between regimes, which is built on the basis of previous analysis. Then, the relationship between spring stiffness and stable region is confirmed in Section 4. Furthermore, the way on how to evaluate the effect of spring stiffness can be obtained. Finally, conclusions are given in Section 5.

2. Statics analysis of the underactuated fingers

In order to obtain the configurations where the finger can realize a stable grasp, this section reviews the statics analysis of the underactuated fingers. Without loss of generality, the model of the underactuated hand with two fingers can be shown in Fig. 1(a), and it has a symmetrical design. Each finger consists of two phalanges L_1 and L_2, and the actuation mechanism of each figure consists of four links a, b, c, and d, wherein link c and phalange L_2 are bounded together with an constant angle ψ, link a and phalange b are connected together with an varied angle γ, and d is a fixed link. The motor torque T_a is actuated with link a, which transfers the actuation torque to the phalanges. T_k is the spring passive torque.

The statics will provide a formulation of the actuating torques and the contact force on the object. The contact force can be expressed as [21]:

$$\mathbf{f} = (\mathbf{J}_0{}^T)^{-1}(\mathbf{J}_1{}^T)^{-1}(\mathbf{J}_2{}^T)^{-1}(\mathbf{J}_3{}^T)^{-1}\mathbf{t}, \tag{1}$$

where $\mathbf{f} = \begin{bmatrix} F_1 & F_2 \end{bmatrix}^{\mathrm{T}}$ is the output expression of the contacted forces exerted on the object, $\mathbf{t} = \begin{bmatrix} T_a & T_k \end{bmatrix}^T$ is the input expression of the active actuating torque and the passive spring torque. Matrix $\mathbf{J_0}$ is the Jacobian matrix of grasp, while matrices $\mathbf{J_1}, \mathbf{J_2}$ and $\mathbf{J_3}$ depend on the driving mechanism used to propagate the actuating torque to the phalanges, i.e.,

$$\mathbf{J}_0 = \begin{bmatrix} p_1 & 0 \\ p_2 + L_1(\cos\theta_2 + \mu\sin\theta_2) & p_2 \end{bmatrix}, \tag{2}$$

where the friction is considered and μ is the coefficient of static friction, variables p_1 $(0 < p_1 < L_1)$ and p_2 $(0 < p_2 < L_2)$ express the contact points' locations defined in Fig. 1.

The matrices $\mathbf{J_1}, \mathbf{J_2}$ and $\mathbf{J_3}$ are expressed as [22]:

$$\mathbf{J}_1 = \begin{bmatrix} 1 & 0 \\ -1 & 1 \end{bmatrix}, \tag{3a}$$

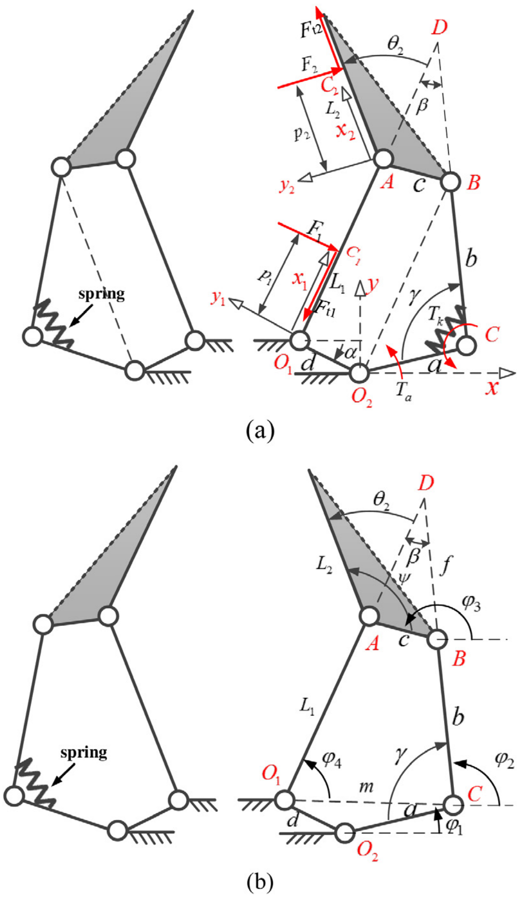

Fig. 1. Model (A) of the two-finger.

$$\mathbf{J}_2=\begin{bmatrix}X_1 & Y_1\\ X_2 & Y_2\end{bmatrix}=\begin{bmatrix}-\dfrac{\partial f_4/\partial\varphi_1}{\partial f_4/\partial\varphi_4} & -\dfrac{\partial f_4/\partial\varphi_2}{\partial f_4/\partial\varphi_4}\\ -\dfrac{\partial f_3/\partial\varphi_1}{\partial f_3/\partial\varphi_3} & -\dfrac{\partial f_3/\partial\varphi_2}{\partial f_3/\partial\varphi_3}\end{bmatrix}, \tag{3b}$$

$$\mathbf{J}_3=\begin{bmatrix}1 & 0\\ 1 & -1\end{bmatrix}, \tag{3c}$$

where f_3 and f_4 are obtained owing to the fingers' closed-loop device, and

$$\begin{aligned}f_3 &= d^2+a^2+b^2+c^2-L_1^2+2da\cos(\alpha-\varphi_1)\\ &\quad+2db\cos(\alpha-\varphi_2)\\ &\quad+2dc\cos(\alpha-\varphi_3)+2ab\cos(\varphi_1-\varphi_2)+2ac\cos(\varphi_1-\varphi_3)\\ &\quad+2bc\cos(\varphi_2-\varphi_3)\end{aligned} \tag{4a}$$

$$\begin{aligned}f_4 &= d^2+a^2+b^2+L_1^2-c^2+2da\cos(\alpha-\varphi_1)\\ &\quad+2db\cos(\alpha-\varphi_2)\\ &\quad-2dL_1\cos(\alpha-\varphi_4)+2ab\cos(\varphi_1-\varphi_2)-2aL_1\cos(\varphi_1-\varphi_4)\\ &\quad-2bL_1\cos(\varphi_2-\varphi_4)\end{aligned} \tag{4b}$$

Hence, one obtains the analytical expressions

$$\mathbf{f}=\begin{bmatrix}\dfrac{(p_2Y_2+L_1Y_1G)T_a+[p_2(X_2+Y_2)+L_1(X_1+Y_1)G]T_k}{p_1p_2(X_1Y_2-X_2Y_1)}\\ -\dfrac{Y_1T_a+(X_1+Y_1)T_k}{p_2(X_1Y_2-X_2Y_1)}\end{bmatrix} \tag{5}$$

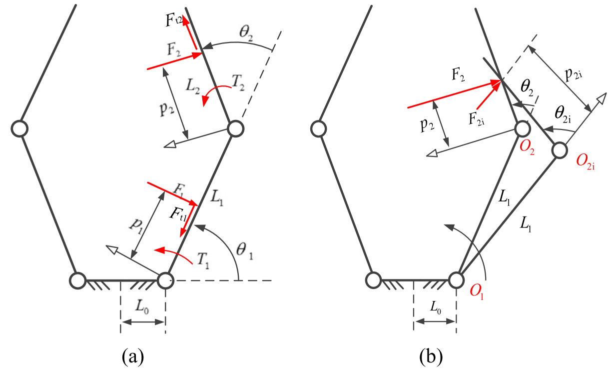

Fig. 2. Model (B) of the two-finger.

where $G=\cos\theta_2+\mu\sin\theta_2$, T_k is related to the spring stiffness K and expressed as

$$T_k=K\bigtriangleup\gamma=K(\gamma-\gamma_0), \tag{6}$$

where γ_0 is the initial value of γ.

For the sake of further analysis, internal torques should be expressed, which can be considered as a series of links redistribute the actuation torque to the joint space (Fig. 2(a)). The parameter of the proximal phalanx's length L_1, distal phalanx L_2, and the palm width L_0 are called as the geometrical parameters in this kind of statics analysis model. The other design parameters of the fingers related to the actuating mechanism are called as the actuation parameters. The actuation mechanism of each figure distributes the active actuating torque T_a and the passive spring T_k to the phalanges, which can be characterized by T_1 (acting on the proximal phalanx) and T_2 (acting on the distal phalanx). The following ratio is defined:

$$R=\frac{T_2}{T_1}. \tag{7}$$

This ratio is not necessarily fixed, but it relies on the actual angle of the joints.

To simplify the calculations, the reference objects' shape is circular, and the object initial location is enforced at the line of symmetry about the palm, so only the right finger is considered. For grasp equilibrium, the net wrench must be zero. However, we consider the situation with force balance only in this paper, the phalanges bring a compressed contact force for the object which is characterized by the radius r_{obj}. The contact forces' amplitude relies on the contact points' position and the distal phalanx's angle [9]:

$$\mathbf{f}=\begin{bmatrix}\dfrac{T_1}{p_1}\left(1-R\left(\dfrac{p_2+L_1G}{p_2}\right)\right)\\ \dfrac{T_1R}{p_2}\end{bmatrix} \tag{8}$$

T_1, T_2 are the identical effects of T_k and T_a combining and dispersing to each joint of the phalanges. Therefore, making corresponding items between Eqs. (5) and (8) equal with each other, one can obtain

$$T_1=\frac{(Y_2-Y_1)T_a+(X_2+Y_2-X_1-Y_1)T_k}{X_1Y_2-X_2Y_1} \tag{9}$$

$$T_2=-\frac{Y_1T_a+(X_1+Y_1)T_k}{X_1Y_2-X_2Y_1} \tag{10}$$

As mentioned above, combining (9) and (10) and substituting (6) yields the spring stiffness

$$K=-\frac{[R(Y_2-Y_1)+Y_1]T_a}{[R(X_2+Y_2-X_1-Y_1)+X_1+Y_1](\gamma-\gamma_0)} \tag{11}$$

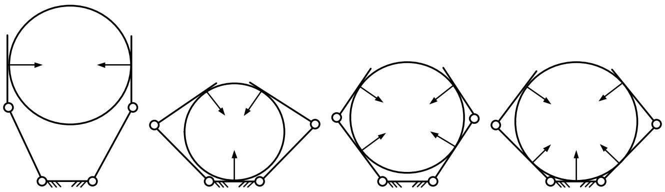

(a) 2-point. (b) 3-point. (c) 4-point. (d) 5-point.

Fig. 3. Different patterns of grasping.

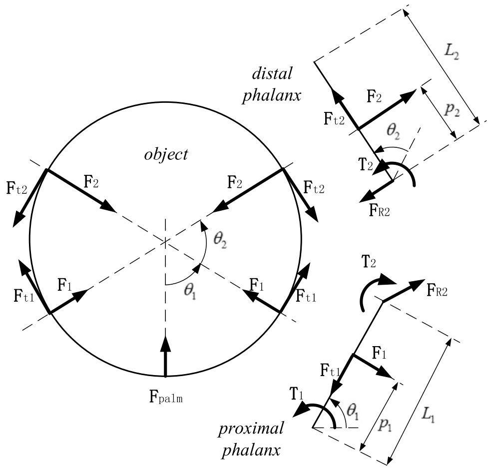

Fig. 4. Free body sketch of the object and the right finger.

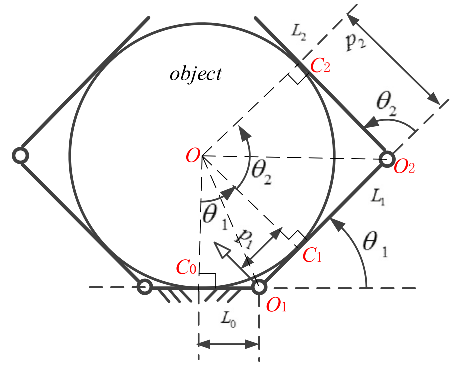

Fig. 5. Geometric relationship in 5-point grasp type.

Notice that the spring is useful for holding the finger with an expected motion. Four different patterns of grasping are illustrated in Fig. 3 including power (3-point, 4-point, 5-point) and pinch (2-point) grasp when R is changed [9]. That is to say, the existence of grasp equilibrium is decided by the spring stiffness. For a planar underactuated gripper composed of two phalanges, it can smoothly adapt to contact forces to different objects in the grasping process, and there will be a stability region where the objects are moved toward to the stable grasping equilibrium. For a grasp process, the contact will still be remained with the distal phalanx by sliding against the object. This sliding proceeding will continue until a force equilibrium stable configuration is achieved, until a stable situation with joint limitation is met (the adaptation of shape is less effective), or until the object is curled away or loosed contact with the last phalanx (ejection). Fig. 4 shows the free body sketch of the object and the right finger, which is in equilibrium, if the resultant of the contact forces is zero.

Only the y-direction's resultant force is considered with the assumption of the symmetric grasp.

$$F_{obj,y} = 2F_1 C_{F_1} + 2F_2 C_{F_2} + F_{palm}, \tag{12}$$

where

$$C_{F_1} = \cos\theta_1 + \mu \sin\theta_1, \tag{13}$$

$$C_{F_2} = \cos(\theta_1 + \theta_2) - \mu \sin(\theta_1 + \theta_2). \tag{14}$$

It is common to emerge a slide by the phalanxes of the finger in contacting with the object, and an balanced position can be attained in the distal phalanx but just for one and unique particular contacting position $p_2 = e$, where e is the location of p_2 at grasp equilibrium, which means the distance between a contact point on a distal phalange and its joint.

5-*point grasp:*

For 5-point grasp type, the object contact with both phalanx and palm, as shown in Fig. 5. According to the geometric relationship ($\Delta OC_0O_1 \cong \Delta OC_1O_1$, $\Delta OC_1O_2 \cong \Delta OC_2O_2$), the equilibrium point can be obtained, i.e.

$$e = L_1 - L_0. \tag{15}$$

4-*point grasp:*

For 4-point grasp pattern, the object lose contact with the palm, so the $F_{palm} = 0$. Substituting $F_{palm} = 0$ and (5) into (14), the equilibrium point can be obtained, i.e.

$$e = \frac{L_1(C_{F_2} - C_{F_1}G)[Y_1T_a + (X_1 + Y_1)T_k]}{(Y_2C_{F_1} + Y_1C_{F_2})T_a + [(X_2 + Y_2)C_{F_1} + (X_1 + Y_1)C_{F_2}]T_k}. \tag{16}$$

3-*point grasp:*

The location of p_2 at grasp equilibrium corresponds to the solution of Eq. (5) ($F_1(p_2) = 0$), i.e.

$$e = -\frac{L_1Y_1T_a + L_1(X_1 + Y_1)T_k}{Y_2T_a + (X_2 + Y_2)T_k} G. \tag{17}$$

2-*point grasp:*

Pinch grasp type has difficulty in achieving stability [23]. Due to the potential energy of the system, the equilibrium point is not local minimum.

In addition, it can be seen that, from the distal phalanx, the contact location will be introduced to analyze whether a sliding motion bring a stable position or not. It can be also easily shown through considering the triangle which is constituted by O_1, O_2, and the contact point (illustrated in Fig. 2(b)), and if this contact location exists and is fixed in space, one has

$$p_2^2 - p_{2i}^2 + 2L_1(p_2\cos\theta_2 - p_{2i}\cos\theta_{2i}) = 0, \tag{18}$$

where p_{2i} and θ_{2i} are an arbitrary initial configuration respectively. This equation formulates that the distance between the finger base point and the location of contact is invariant for any pair (p_{2i}, θ_{2i}). The contact curves can be tracked in the (p_2, θ_2) plane, which was regarded as the grasp-state plane [3], examples with certain parameters will be illustrated in Section 4.

From (18), the finger has one DOF while it is in contaction with the object. This motion can be precisely described and referred to as a self-adaptive motion. Indeed, the contacting trajectory is a curve in the contacting plane (p_2, θ_2), and if the contacting trajectory crosses an equilibrium curve, the grasp will finally stable, otherwise the contact with the object will be lost, namely due to the kinematic evolution, one obtains the ejection phenomenon.

In conclusion, depending on the contact trajectory (18) and the equilibrium curve (15)–(17), different final stability region can be obtained by defining different parameters of the mechanism including geometric parameters and spring stiffness and so on.

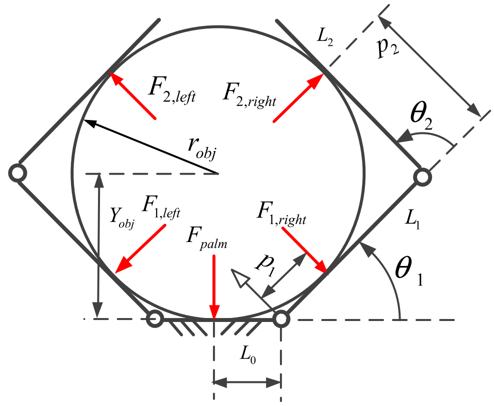

Fig. 6. Scheme of an underactuated gripper.

3. Bifurcations between grasps of different topology

From the statics analysis above, one can attain the function of spring stiffness K and express the stable region for a two-finger underactuated hand. Due to the performance of the stabilization affected by spring stiffness, the relationship between spring stiffness and stable region needs to be confirmed. Beyond that, the spring stiffness's delimiter between regimes should be figured out to make sure the spring is appropriate for the underactuated finger, and it can be attained based on (11) by analyzing the radius of grasped object and the value of R in different grasp type. The method to analyze the value of radius and R in different grasp type in based on [9] and presented by following.

3.1. The range of object sizes under various grasp types

When the underactuated finger makes contact with an object, various mechanism characteristic parameters lead to various object sizes and contact points. As illustrated in Fig. 4, two constraint equations describing contact between phalanges of the right finger and the object are as follows [9]:

$$\begin{pmatrix} L_0 + p_1 \cos\theta_1 \\ p_1 \sin\theta_1 \end{pmatrix} = \begin{pmatrix} r_{obj} \sin\theta_1 \\ Y_{obj} - r_{obj}\cos\theta_1 \end{pmatrix} \tag{19}$$

$$\begin{pmatrix} L_0 + L_1\cos\theta_1 + p_2\cos(\theta_1+\theta_2) \\ L_1\sin\theta_1 + p_2\sin(\theta_1+\theta_2) \end{pmatrix} = \begin{pmatrix} r_{obj}\sin(\theta_1+\theta_2) \\ Y_{obj} - r_{obj}\cos(\theta_1+\theta_2) \end{pmatrix} \tag{20}$$

where Y_{obj} is the distance between the object's center and the palm ($Y_{obj} = r_{obj}$), θ_1 is the proximal joint's rotation with respect to the palm, and other signs were defined in Section 2. Equation of the left finger is similar but mirrored with regard to the vertical axis (see Fig. 6).

5-point grasp mode:

For a 5-point grasp mode, the equations (Eqs. (19), (20)) and $Y_{obj} = r_{obj}$ must be satisfied. Such a grasp mode can only exist if:

$$L_0 \le L_1 \le L_0 + L_2. \tag{21}$$

As shown in Fig. 5, the magnitude of θ_1 and θ_2 is deduced by applying the cosine rule, which can be attained that:

$$\cos\theta_1 = \frac{r_{obj}^2 - L_0^2}{r_{obj}^2 + L_0^2}, \tag{22}$$

$$\cos\theta_2 = \frac{r_{obj}^2 - (L_1 - L_0)^2}{(L_1 - L_0)^2 + r_{obj}^2}. \tag{23}$$

Substituting Eq. (22) and $\theta_1+\theta_2 = \pi/2$ into Eq. (20) and the grasped object sizes with 5 contact points is yielded through solving for r_{obj}

$$r_{obj,5} \le \frac{1}{2}\left(L_1 + \sqrt{L_1^2 - 4L_0^2 + 4L_0L_1}\right). \tag{24}$$

4-point grasp mode:

For the 4-point grasp mode, Eqs. (19) and (20) are satisfied with $Y_{obj} > r_{obj}$. This grasp mode can only exist if:

$$L_1 > L_0. \tag{25}$$

The object sizes in this grasp type is:

$$r_{obj,4} \le \begin{cases} \frac{1}{2}\left(L_1 + \sqrt{L_1^2 - 4L_0^2 + 4L_0L_1}\right) & \text{if } L_0 \le L_1 \le L_0 + L_2 \\ \sqrt[3]{H_1 + \sqrt{H_1^2 + H_2^3}} \\ \quad + \sqrt[3]{H_1 - \sqrt{H_1^2 + H_2^3}} + \frac{1}{3}L_0 & \text{if } L_1 > L_0 + L_2 \end{cases} \tag{26}$$

where

$$H_1 = \frac{1}{27}L_0(L_0^2 + 9L_1L_2 + 9L_2^2), \tag{27}$$

$$H_2 = \frac{1}{3}L_2(-2L_1 + L_2) - \frac{1}{9}L_0^2. \tag{28}$$

3-point grasp mode:

With the 3-point grasp mode, only the constraint equation of the distal phalanx (20) has to be satisfied. Such a grasp mode can only exist if [9]:

$$L_1 \le L_0 + L_2 \tag{29}$$

The largest grasped object with this mode is obtained by substituting $Y_{obj} = r_{obj}$ and $\theta_1 + \theta_2 = \pi/2$ into (20) (because when the fingers are splaying to the greatest degree in a 3-point grasp mode, it is in a critical state of the 2-point grasp type, and the requirement about $\theta_1 + \theta_2 = \pi/2$ is workable at this situation). Solving it for r_{obj} and θ_1 yields:

$$r_{obj} \le \begin{cases} L_0 + L_1 & \text{if } L_1 \le L_2 - L_0 \\ \frac{1}{2}\left(L_2 + L_0 + \sqrt{2L_1^2 - (L_2 - L_0)^2}\right) & \text{if } L_2 - L_0 < L_1 \le L_0 + L_2 \end{cases} \tag{30}$$

2-point grasp mode:

For the 2-point grasp mode, the maximal object size corresponds to the results of $r_{obj,3}$ and $r_{obj,4}$:

$$r_{obj,2} < \begin{cases} r_{obj,3} & \text{if } L_1 \le L_0 + L_2 \\ r_{obj,4} & \text{if } L_1 > L_0 + L_2 \end{cases} \tag{31}$$

The object smaller than $r_{obj,2}$ can be grasped with 2-point grasp mode, while $L_1 < L_0$. Then the object size should satisfy:

$$r_{obj,2} > \begin{cases} L_0 - L_1 & \text{if } L_1 \le L_0 + L_2 \\ 0 & \text{if } L_1 > L_0 + L_2 \end{cases} \tag{32}$$

Therefore, based on the geometric parameters of the finger's link, as well as the contact points between the object and the phalanges, one can attain the maximum grasped object size. Then, to achieve the static equilibrium of the system with a 3-point grasp, the rate of the finger's actuation torques should be analyzed as it is not determined yet.

Through (8), the existence of grasp equilibrium and the amount of the contact points are determined by R. If R increases, the

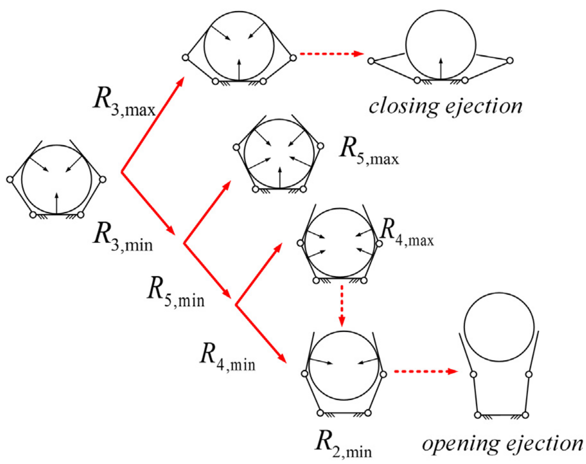

Fig. 7. Bifurcations between various grasp types.

magnitude of F_2 will also increase whereas F_1 will decrease. The object will be pushed against the palm. If R further increases, F_1 will become zero, the phalanx will lose contact, and the contacting point on the distal phalanx will move toward to the finger's tip. In addition to the situation of stability, two different types of ejection namely opening- and closing-ejection have been identified [11].

3.2. The transition of various grasp types

When the underactuated fingers grasp an object, the grasp type is not fixed until the grasp is completed. Observations of Eqs. (8), (12) shows that the number of contact points is determined by R. There will be a transition of various grasp types when R is increased or decreased, as shown in Fig. 5. For different grasp types, the range of R is different. The range of R for different grasp types are discussed in the following (see Fig. 7).

5-point grasp mode:

When an object is grasped in a 5-point grasp, the geometric relations are determined, as shown in Fig. 5. The $\cos\theta_1$ and $\cos\theta_2$ are given in Eqs. (22), (23), and $\sin\theta_1$ and $\sin\theta_2$ can be found that:

$$\sin\theta_1 = \frac{2L_0 r_{obj}}{r_{obj}^2 + L_0^2}, \tag{33}$$

$$\sin\theta_2 = \frac{2(L_1 - L_0)r_{obj}}{(L_1 - L_0)^2 + r_{obj}^2}, \tag{34}$$

When R approaches the upper limit $R_{5,max}$, the proximal phalanges' contact force becomes zero, which can be obtained from (8):

$$1 - R\left(\frac{p_2 + L_1(\cos\theta_2 + \mu\sin\theta_2)}{p_2}\right) = 0. \tag{35}$$

Solving the equations Eqs. (19), (20) with $Y_{obj} = r_{obj}$, and Eq. (35), the $R_{5,max}$ can be attained:

$$R_{5,max} = \frac{L_1 - L_0}{L_1 - L_0 + L_1(\cos\theta_2 + \mu\sin\theta_2)}. \tag{36}$$

When the R approaches the lower limit $R_{5,min}$, the contacting force between the object and palm becomes zero. Solving Eqs. (19), (20) with $Y_{obj} = r_{obj}$, and Eq. (12) with $F_{palm} = 0$, the $R_{5,\min}$ can be deduced:

$$R_{5,min} = \begin{cases} > 0 & \text{if } r_{obj} \le L_0 \\ \dfrac{(L_1 - L_0)c_{F_1}}{(L_1 - L_0 + L_1(\cos\theta_2 + \mu\sin\theta_2))\,c_{F_1} - L_0 c_{F_2}} & \text{if } r_{obj} > L_0 \end{cases} \tag{37}$$

4-point grasp mode:

At the upper limit $R_{4,\max}$,

$$R_{4,max} = R_{5,min} \quad \text{if } L_1 \le L_0 + L_2. \tag{38}$$

When $L_1 > L_0+L_2$, the upper limit is caused by the closing ejection.

At the lower limitation $R_{4,min}$, the fingers envelope the object ($\theta_1+\theta_2 = \pi/2$). Solving Eqs. (19), (20) with $\theta_1+\theta_2 = \pi/2$, it can be attained:

$$\cos\theta_1 = \sin\theta_2 = \frac{r_{obj} - L_0}{L_1}, \tag{39}$$

$$\sin\theta_1 = \cos\theta_2 = \frac{\sqrt{L_1^2 - (r_{obj} - L_0)^2}}{L_1}, \tag{40}$$

$$p_2 = r_{obj}\tan\frac{\theta_2}{2} = \frac{r_{obj}\left(L_1 - \sqrt{L_1^2 - (r_{obj} - L_0)^2}\right)}{r_{obj} - L_0}, \tag{41}$$

Thus, $R_{4,\min}$ can be attained according to Eq. (12) with $F_{palm} = 0$

$$R_{4,min} = \frac{p_2(c_{\theta_1} + \mu s_{\theta_1})}{(p_2 + L_1(c_{\theta_1} + \mu s_{\theta_1}))\,(c_{\theta_1} + \mu s_{\theta_1}) + \mu(L_1 - p_2)}. \tag{42}$$

3-point grasp mode:

As for the 3-point grasp mode, the distal phalanges constrict the object against the palm, and the proximal contact force becomes zero (Eq. (35)).

When R reaches the upper limit $R_{3,\max}$, with constraint conditions of $L_1 > L_2 - L_0$ and $L_1 > L_0$, the contact point is located on the distal phalanges' tip where $p_2 = L_2$ or with constraint conditions of $L_1 \le L_2 - L_0$, the upper limitation is deduced by the boundary condition that $\theta_1 \ge 0$. Respectively, one can obtain the following analytical equation according to Eq. (35):

$$R_{3,max} = \frac{p_2}{p_2 + L_1(\cos\theta_2 + \mu\sin\theta_2)}. \tag{43}$$

If $L_1 \le L_2 - L_0$, the upper limit occurs when $\theta_1 = 0$. In this situation, the condition $p_2 = L_0 + L_1$ is satisfied. Solving Eqs. (19), (20) with $\theta_1 = 0$, $p_2 = L_0 + L_1$ and $Y_{obj} = r_{obj}$, the following equations can be attained:

$$\cos\theta_2 = \frac{r_{obj}^2 - (L_0 + L_1)^2}{r_{obj}^2 + (L_0 + L_1)^2}, \tag{44}$$

$$\sin\theta_2 = \frac{2r_{obj}(L_0 + L_1)}{r_{obj}^2 + (L_0 + L_1)^2}. \tag{45}$$

If $L_1 > L_2 - L_0$ and $L_1 \ge L_0$, the upper limit occurs when $p_2 = L_2$. Substituting $p_2 = L_2$ and $Y_{obj} = r_{obj}$ into Eqs. (19), (20), it can be attained that:

$$\cos\theta_2 = \frac{L_2(L_0^2 - L_1^2 - L_2^2) + r_{obj}H_3}{2L_1(L_2^2 + r_{obj}^2)}, \tag{46}$$

$$\sin\theta_2 = \frac{r_{obj}(-L_0^2 + L_1^2 + L_2^2) - L_2H_3}{2L_1(L_2^2 + r_{obj}^2)}, \tag{47}$$

where

$$H_3 = \sqrt{-(L_0^2 - L_1^2 - L_2^2)^2 + 4L_1^2(L_2^2 + r_{obj}^2)}. \tag{48}$$

When R reaches the lower limit $R_{3,\min}$, the proximal phalanges move to touch the object or the contact force between the palm and the object becomes zero ($F_{palm} = 0$). It is determined by the object size whose contact point is lost. As illustrated in Fig. 5, the first situation is actually transform to a 5-point grasp mode (i.e. $R_{3,\min} = R_{5,\max}$); the second situation is the transform to a 2-point grasp mode or opening ejection. For the second scenario, to obtain an analytical expression of $R_{3,\min}$, substitute $Y_{obj} = r_{obj}$ into (20) and (35), respectively, with a requirement of $0 < \theta_1 < \pi$, and one can obtain the following analytical equations:

$$\cos\theta_2 = \sqrt{1 + \frac{-L_0^2 - 2L_0 r_{obj} + 2r_{obj}H_4 - r_{obj}(1+2\mu^2)}{L_1^2(1+\mu^2)}}, \tag{49}$$

$$\sin\theta_2 = \frac{L_1^2 r_{obj}^2(1+\mu)^2 - H_4}{L_1^3 r_{obj}(1+\mu^2)^2}, \tag{50}$$

$$p_2 = \frac{-L_0\mu H_5 - L_1^3 r_{obj}^2 \mu H_6 + r_{obj}\left(H_5 - L_0 L_1^3 H_6\right)}{L_1^2 r_{obj}(L_0 + r_{obj}\mu)(1+\mu^2)^2}, \tag{51}$$

where

$$H_4 = \sqrt{(L_0 + r_{obj}\mu)(1+\mu^2)}, \tag{52}$$

$$H_5 = \sqrt{L_1^4 r_{obj}^2 (L_0 + r_{obj}\mu)(1+\mu)^3}, \tag{53}$$

$$H_6 = (1+\mu^2)^2\cos\theta_2, \tag{54}$$

Thus the $R_{3,min}$ can be obtained according to (29):

$$R_{3,min} = \begin{cases} R_{5,max} & \text{if } r_{obj} \le r_{obj,5} \\ \dfrac{p_2}{p_2 + L_1(\cos\theta_2 + \mu\sin\theta_2)} & \text{if } r_{obj} > r_{obj,5} \end{cases} \tag{55}$$

where $r_{obj,5}$ is defined by Eq. (24).

2-point grasp mode:

As for 2-point grasp mode, the object touches the distal phalanges only (Eq. (35)) and the object lose contact with the palm ($Y_{obj} > r_{obj}$ and $F_{palm} = 0$). When the R approaches the upper limit $R_{2,\max}$, the contact point is at the distal phalanx's tip ($p_2 = L_2$). Substituting $F_{palm} = 0$ and $p_2 = L_2$ into Eqs. (35) and (20), the following equations can be attained:

$$\cos\theta_2 = \frac{L_1^2\mu H_8 - L_0 L_1 \mu H_7 - \sqrt{-L_1^2(1+\mu^2)H_7 H_9}}{L_1^3(r_{obj} - L_2\mu)(1+\mu^2)^2}, \tag{56}$$

$$\sin\theta_2 = \frac{L_1^2 H_8 - L_0 L_1(1+\mu^2)H_7 + \mu\sqrt{-L_1^2(1+\mu^2)H_7 H_9}}{L_1^3(r_{obj} - L_2\mu)(1+\mu^2)^2}, \tag{57}$$

where

$$H_7 = \sqrt{L_1^2(r_{obj} - L_2\mu)^2(1+\mu^2)}, \tag{58}$$

$$H_8 = (r_{obj} - L_2\mu)^2(1+\mu^2), \tag{59}$$

$$H_9 = \sqrt{\frac{L_0^2 L_1(1+\mu^2) - 2L_0 H_7 + L_1\left((r_{obj} - L_2\mu)^2 - L_1^2(1+\mu^2)\right)}{L_1}}. \tag{60}$$

Thus, the $R_{2,\max}$ can be obtained according to Eq. (35):

$$R_{2,max} = \frac{L_2}{L_2 + L_1(\cos\theta_2 + \mu\sin\theta_2)}. \tag{61}$$

At the lower limit $R_{2,\min}$, the object is very close to contact the proximal phalanges or the palm. The first situation is actually a transform to the 4-point grasp mode, and the second situation is a transform to the 3-point grasp mode. According to that, the $R_{2,\min}$ can be determined as:

$$R_{2,min} = \begin{cases} > 0 & if \;\; r_{obj} \le L_0 \\ R_{4,min} & if \;\; L_0 < r_{obj} < r_{obj,5} \\ R_{3,min} & if \;\; r_{obj} \ge r_{obj,5} \end{cases} \tag{62}$$

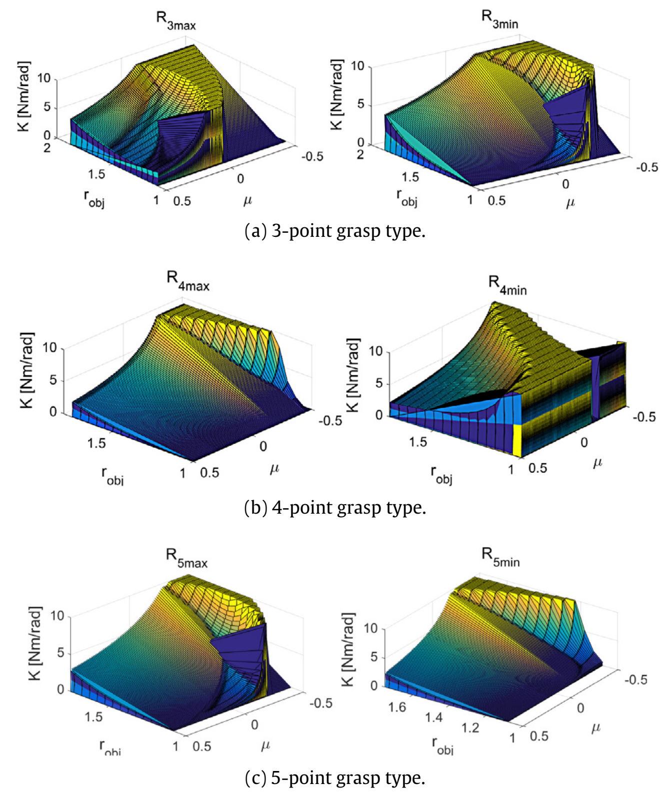

(a) 3-point grasp type.

(b) 4-point grasp type.

(c) 5-point grasp type.

Fig. 8. Relationship between K, r_{obj} and μ.

The previous analysis on R can be seen as a formulation of the geometric parameters and the maximum object size. Note that the term γ is the functions of θ_2. Hence, as shown in Eq. (11), when R is regarded as constant and the range of θ_2 is confirmed, the spring stiffness K is related to the angle γ. That is to say, R and θ_2 decide the extent of the envelope grasping, which means the contact points' number and locations. If the designer confirms the size of an object and the extent of the envelope grasping, the range of spring stiffness K can be obtained.

4. A metric to design spring stiffness

4.1. The ranges of spring stiffness

According to Eq. (11), the stiffness of spring can be expressed by R, γ, T_a and the geometric parameter of the finger. The parameter γ related to the pose of the fingers, and the pose usually depends on the radius of the grasped object. The input torque T_a is a parameter one can control. To have a better understanding for evaluating the spring stiffness, without losing the generality, the value of T_a is given as 1 N m. The ranges of R and radius of object in different grasp type have been analyzed in Section 3. And also the maximal R and minimal R in different grasp type have been attained in Section 3, which rely on the radius of the grasped object. Based on that, the relationships between K, friction and radius of grasped object in different grasp type are attained and presented in Fig. 8.

The spring stiffness in maximal R are shown in the left figures, while the spring stiffness in minimal R are shown in the right figures. The ranges of the spring stiffness is the value between the stiffness in maximal R and the stiffness in minimal R. The spring stiffness should be design to satisfy the ranges of the stiffness.

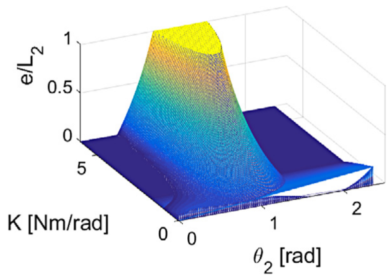

Fig. 9. The equilibrium curves in 3-point grasp type.

Table 1
Geometric parameters.

L_0	L_1	L_2	ψ	A	b	c	γ_0
0.5	1.5	2	120°	0.8	1.1	0.6	90°

4.2. *Relationship between spring stiffness and stable region based on grasp-state plane*

This subsection will focus on a graphical method with associated metric on the relationship between spring stiffness and the size of the stable region. The 3-point grasp mode, the 4-point grasp mode and the 5-point grasp mode will be discussed in the following. Because that 2-point grasp mode is critical stable, so this grasp type is not discussed any more in the following discussion. According to (15)–(17), the equilibrium point depends on the input torque T_a, the stiffness K, the object's radius and the finger's geometric parameters. Giving the condition of $T_a = 1$ N m, $r_{obj} = 1.5$ and the geometric parameters presented in Table 1, the equilibrium point can be expressed by the stiffness K and angle θ_2, which are shown in Figs. 9, 12 and 15, where e/L_2 means the relative position of contacting point on the distal phalange, and it is the phalange's physical condition for successfully grasping an object.

3-point grasp mode:

Fig. 9 shows the equilibrium curves in 3-point grasp type (Eq. (17)). Note that Fig. 9 includes two different types of equilibrium curves: the one truncated by geometer restrain (L_2) and the integrity one, which lead to two types of stability regions.

The stability regions shows in Fig. 10 with different static coefficient of friction ($\mu = \pm 0.2$, $\mu = \pm 0.5$). The stability regions, as shown in Fig. 10(a) and (b), can be attained under the following steps. Firstly, the point of intersection (θ_{i2}) between equilibrium curve (17) and contact trajectory (18) whose slopes are equal should be found. Then, these two kinds of curves together with geometer restrain ($0 < p_2 < L_2$) would form a closed curve. S_i is the area of the stability region, which corresponds to the white area, and can be calculated as follows:

$$S_i = \int_{\theta_{i1}}^{\theta_{i2}} f(\theta_{2i}) d\theta_2 + \int_{\theta_{i2}}^{\theta_{i3}} g(\theta_{2i}) d\theta_2 + \int_{\theta_{i3}}^{\arccos(-\frac{L_2}{2L_1})} d\theta_2 - \int_{\frac{\pi}{2}}^{\arccos(-\frac{L_2}{2L_1})} g(\theta_{2i}) d\theta_2 \tag{63}$$

where θ_{ik} ($k = 1, 2, 3$) represent the changes of the angle θ_2, and θ_{i1} is the point between equilibrium curve and geometer restrain that is located at $p_2 = 0$; θ_{i2} is intersection point as above; θ_{i3} is the point between the contact trajectory and geometer restrain that is located at $p_2 = L_2$. In addition, $g(\theta_{2i})$ is the segment of contact

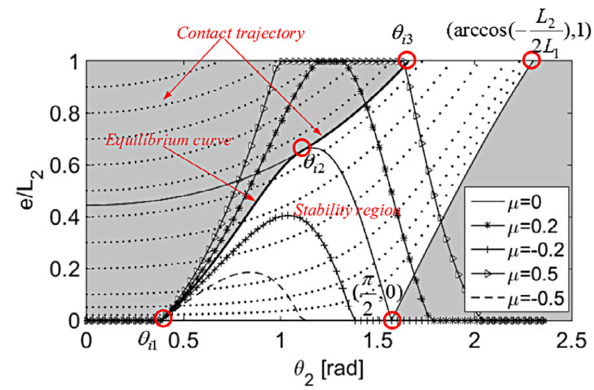

(a) $K = 3$.

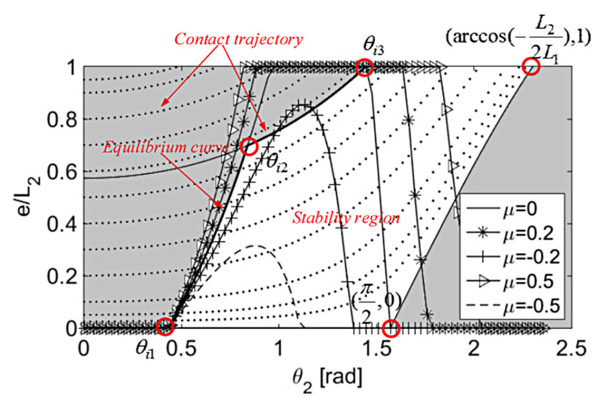

(b) $K = 5$.

Fig. 10. Stability regions with different parameters.

trajectory (18) between θ_{i2} and θ_{i3} in the grasp-plane, which is defined as follows

$$g(\theta_{2i}) = \frac{p_2}{L_2} = \frac{\sqrt{p_i^2 + 2p_i L_1 \cos\theta_{2i} + L_1^2 \cos^2\theta_2} - L_1 \cos\theta_2}{L_2} \tag{64}$$

where $f(\theta_{2i})$ is the segment of equilibrium curve (17) between θ_{i2} and θ_{i3} in the grasp-plane, which is defined as follows

$$f(\theta_{2i}) = \frac{e}{L_2} = \frac{-\frac{L_1 Y_1 T_a + L_1 (X_1 + Y_1) T_k}{Y_2 T_a + (X_2 + Y_2) T_k} G}{L_2}. \tag{65}$$

Therefore, according to (63), the contrast of Fig. 10(a) and (b) is shown that same geometric parameters with different spring stiffness will deduce different stability region. In other words, as shown in Fig. 10, the equilibrium curves are the intersecting surfaces of Fig. 9, and the stability regions are the visualization of (63) to express the relation between the spring stiffness and the stable region.

Corresponding to different spring stiffness, various stability regions as shown in Fig. 10 can be calculated by (63). Thus, one can obtain a curve about the relationship between spring stiffness and stability regions as shown in Fig. 11. If the spring stiffness is too soft, the grasp would become less stabilized, and the stability region (soft interval) would become small as well. If the spring is too stiff, the finger would be similar to a fully actuated one, even the performance of stabilization would get better for some objects with specified size, and it would not be suitable for the majority. As a result, the performance of adaptability would degenerate and the stability region (stiff interval) will also become small. Thus, the spring shall be designed with a moderate stiffness. In a practical

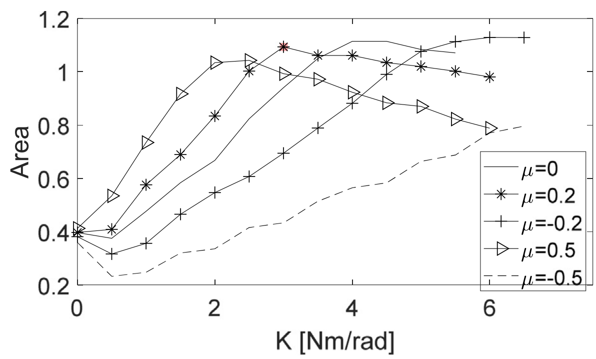

Fig. 11. Area of stability region in 3-point grasp type.

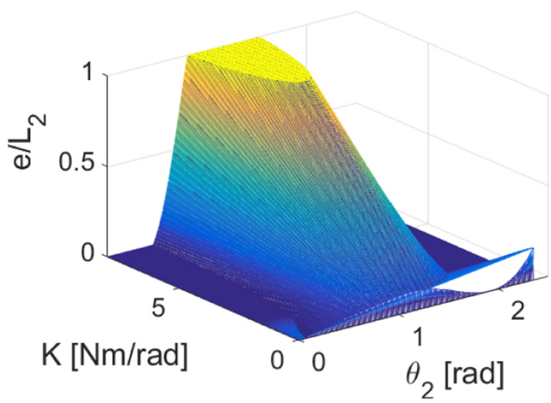

Fig. 12. The equilibrium curves in 4-point grasp type.

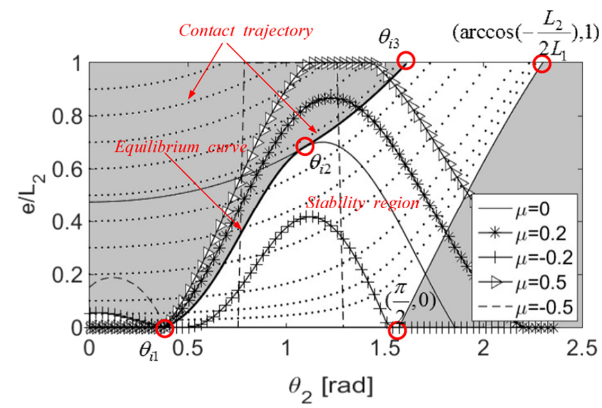

(a) $K = 3$.

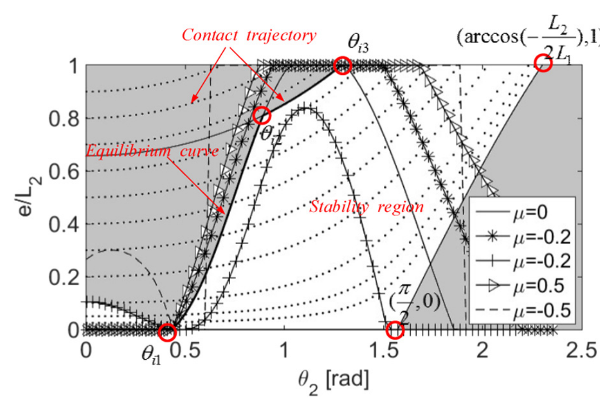

(b) $K = 5$.

Fig. 13. Stability regions with different parameters.

application, it is a guideline to choose the appropriate K, which can affect the trade off between the ability of adaptive to the object and the stability of grasp.

4-*point grasp mode:*

Fig. 12 shows the equilibrium curves in 4-point grasp type (Eq. (16)). The distal phalanx is just considered to attain the area of stability region.

Similar to the method of the 3-point grasp type, the intersecting surfaces of Fig. 12 and the contact trajectory (18) are shown in Fig. 13 with different friction.

Variable stability regions are shown in Fig. 13. Similar to the 3-point grasp, there are two different type stability regions. One type of stability regions is shown in Fig. 13(a), and another type of stability regions is shown in Fig. 13(b), its areas of stability region can be attained by Eq. (63).

Considering the variable friction, the relationship between the spring stiffness and the stability regions is shown in Fig. 14.

5-*point grasp mode:*

As shown in Fig. 15, the equilibrium curves (18) in 5-point grasp type is constant which relies on the mechanism parameters (L_0, L_1). Therefore, it is difficult to find the relationship between spring stiffness and stability regions like 3-point grasp mode and 4-point grasp mode.

In this subsection, the relationships between spring stiffness and stability regions in 3-point grasp mode and 4-point grasp mode are attained, as shown in Figs. 11 and 14. A spring stiffness should be design to maximize the area of stability regions. However, there is a delimiter of stiffness determined by Eq. (11), which must be taken into consideration to design the stiffness.

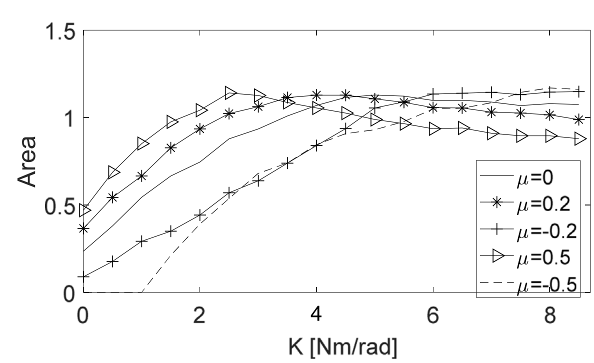

Fig. 14. Area of stability region in 4-point grasp type.

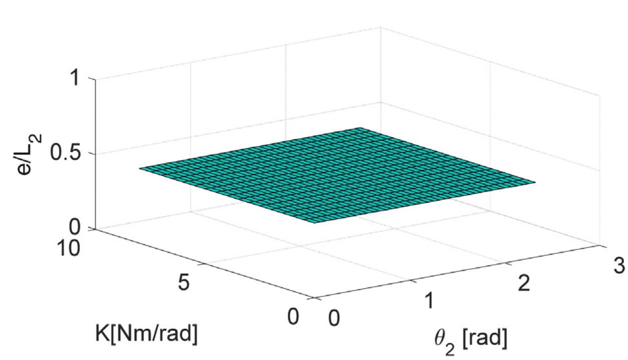

Fig. 15. The equilibrium curves in 5-point grasp type.

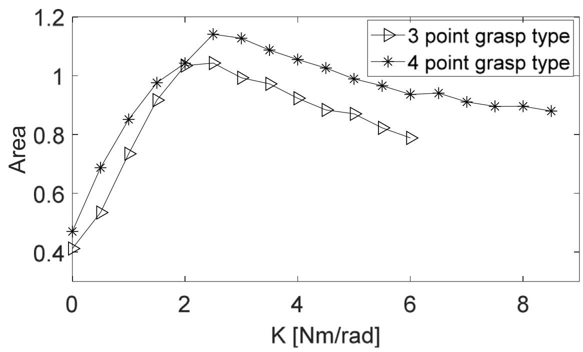

Fig. 16. The area of stability regions.

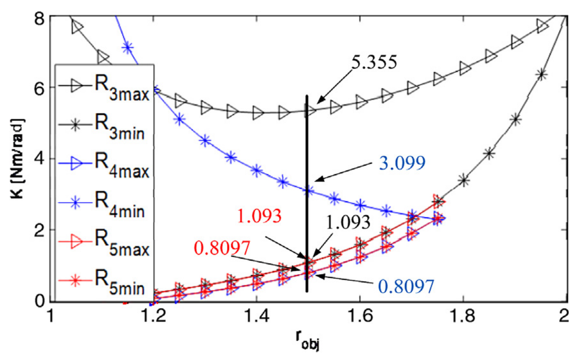

Fig. 17. The ranges of the spring stiffness.

5. A numerical example to design spring stiffness

A rule to design the spring stiffness given in Section 4.1 is that the stiffness should satisfy the ranges of the stiffness. Another rule to design the spring stiffness given in Section 4.2 is that stiffness maximizes the area of stability regions. This two rules give a metric to achieve appropriate spring stiffness. An example to design a spring stiffness is presented by following.

Considering the $\mu = 0.5$ and the $r_{obj} = 1.5$ with $T_a = 1$ N m, the area of stability regions is shown in Fig. 16 and the ranges of stiffness is shown in Fig. 17.

There are three types of ranges of spring stiffness in Fig. 17. First type is with upper limit 1.093 and lower limit 0.8097, which lead to the 5-point grasp type. Second type is with upper limit 3.099 and lower limit 0.8097, which leads to the 4-point grasp type. The last one is with upper limit 5.355 and lower limit 1.093, which leads to the 3-point grasp type. A proper spring stiffness is the one which not only satisfies the ranges of the spring stiffness, but also maximize the area of stability regions. As shown in Fig. 18, the stiffness range of 2.5–3 maximize the area of stability regions in 4 point grasp type. The stiffness range of 2–2.5 maximize the area of stability regions in 3 point grasp mode. Thus, for the 4 point grasp mode, the stiffness in the range of 2.5–3 is the optimal selection. For the 3 point grasp type, the stiffness in the range of 2–2.5 is the optimal. For the 5 point grasp mode, the equilibrium curves rely on the mechanism parameters (as shown in Fig. 15), thus the stiffness in the range of 0.8097–1.093 can be chosen arbitrary.

A metric to design the spring stiffness is presented in this subsection with the fixed value of T_a, μ and r_{obj}. When the finger grasp an object, the μ and r_{obj} are known and constant. The input torque T_a is a artificial control parameter. In order to show the effect of T_a on spring stiffness, the design results with different T_a are presented as following.

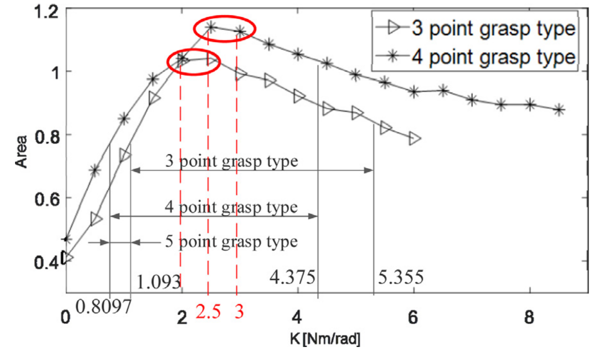

Fig. 18. The results of the evaluation.

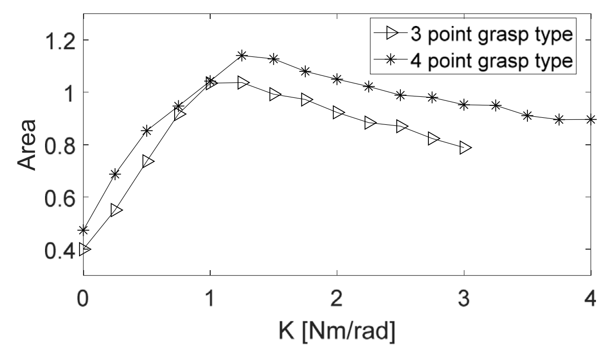

Fig. 19. The area of stability regions.

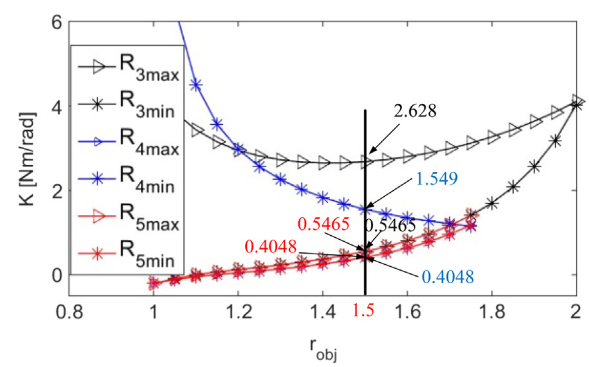

Fig. 20. The ranges of the spring stiffness with $T_a = 0.5$ N m.

Considering another condition of $T_a = 0.5$ N m, then, the corresponding ranges of stiffness is shown in Fig. 19, and the design result is presented in Fig. 20. It can be seen that, for the 4 point grasp mode, the stiffness in the range of 1.25–1.5 is the optimal. For the 3 point grasp mode, the stiffness in the range of 1–1.25 is the optimal. For the 5 point grasp mode, the stiffness in the range of 0.4068–0.5465 can be chosen arbitrary (see Fig. 21).

Considering the condition of $T_a = 1.5$ N m, then, the corresponding ranges of stiffness is shown in Fig. 22, and the design result is presented in Fig. 23. From these figures, it can be seen that, for the 4 point grasp type, the stiffness in the range of 3.5–4.5 is the optimal selection. For the 3 point grasp mode, the stiffness in the range of 3–3.5 is the optimal. For the 5 point grasp type, the stiffness in the range of 1.215–1.639 can be chosen arbitrary.

In this way, an optimal spring stiffness is attained according to the proposed method by giving the particular conditions. The procedure and algorithm is as follows:

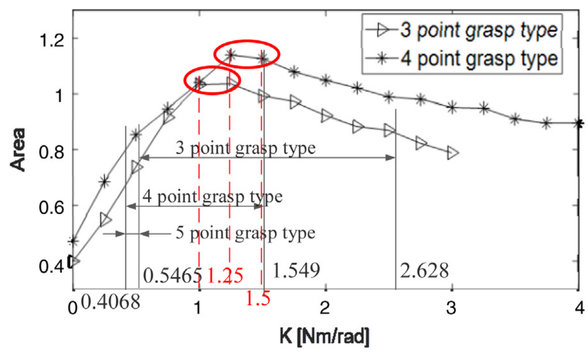

Fig. 21. The results of the evaluation with $T_a = 0.5$ N m.

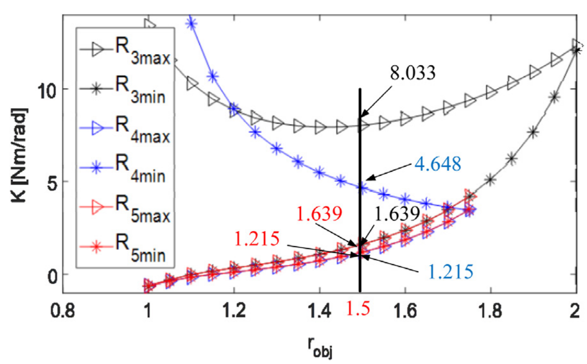

Fig. 22. The ranges of the spring stiffness with $T_a = 1.5$ N m.

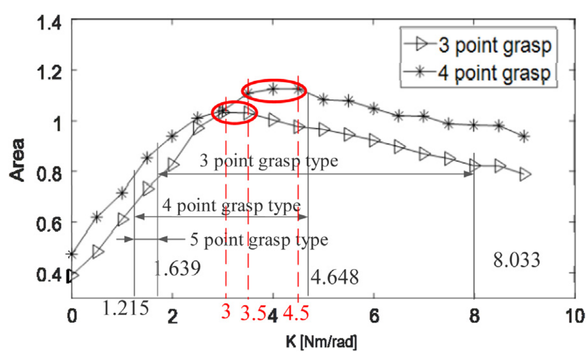

Fig. 23. The results of the evaluation with $T_a = 1.5$ N m.

Inputs:
(1) The input torque: T_a.
(2) The mechanism parameters: L_0, L_1, L_2, a, b and c.
(3) The static friction's coefficient: μ.
(4) The grasped object's radius: r_{obj}.
Outputs: the optimal spring stiffness.
Procedure:
***Step* 1**:

According to Eq. (11), establishing the relationship between the spring stiffness K, the static friction's coefficient μ and the grasped object's radius r_{obj}.

***Step*2**:

For an object, one can know the μ and r_{obj}. Thus the ranges of K can be calculated by the relationship obtained from the *Step*1.

***Step*3**:

Calculating the relationship between the area of stability regions and the spring stiffness K according to Eq. (63).

***Step*4**:

Finding the value of K (or a range of K) from ranges of K (*Step*2) which maximize the area of stability regions. Thus, the optimal spring stiffness is obtained.

In addition, comparing the design results with $T_a = 1$ N m, 0.5 N m and 1.5 N m, one can see that the evaluation of stiffness with $T_a = 1.5$ N m is the maximal and the evaluation of stiffness with $T_a = 0.5$ Nm is the minimum. From that, one can know that the spring stiffness relies on the input torque T_a. In fact, there is a balance between the input torque T_a, contact force $\mathbf{f}$ and the spring torque T_k, as shown in Eq. (5), and the T_k can be expressed by $T_k = K \triangle\gamma$ (as shown in Eq. (6)). The contact force $\mathbf{f}$ and spring torque T_k will increase when the input torque T_a increase, and a larger spring stiffness K is necessary because a small spring stiffness K may lead to excessive rotation of γ, which cause an unstable grasp. However, it is difficult to find the specific relationship between the T_a and K based on the statics analysis. Future work will focus on seeking an analytical interpretation between the T_a and K through dynamic method and so on.

6. Conclusion

This paper presents a metric to achieve appropriate spring stiffness for underactuated fingers. To simplify the analysis, the shape of the reference objects is circular. Based on statics analysis, this method can quantify and visualize the relationship between the spring stiffness and stable region according to grasp-state plane together with the spring stiffness's delimiter between regimes. Then, the grasp stabilization with respect to spring stiffness could be evaluated in a quantitative way by analytical equations and graphs, meanwhile objects are enveloped adaptability to some extent. Finally, an application is presented to design the optimal spring stiffness based on the proposed method by giving the particular conditions. Future wok will focus on implementing experiments to test the verification of the approach.

Acknowledgments

This work was jointly supported by the National Science Foundation of China (Grant Nos. 61773028, 51375034), Natural Science Foundation of Beijing (4172008) and the Fundamental Research Funds for the Central Universities (YWF-17-BJ-J-78).

References

[1] D. Prattichizzo, M. Malvezzi, M. Gabiccini, A. Bicchi, On the manipulability ellipsoids of underactuated robotic hands with compliance, Robot. Auton. Syst. 60 (2012) 33–346.
[2] Wu LiCheng, Giuseppe Carbone, Marco Ceccarelli, Designing an underactuated mechanism for a 1 active DOF finger operation, Mech. Mach. Theory 44 (2009) 336–348.
[3] L. Birglen, T. Laliberte, C. Gosselin, Underactuated Robotic Hands, Springer-Verlag, 2008.
[4] A.M. Dollar, R.D. Howe, The highly adaptive sdm hand: Design and performance evaluation, Int. J. Robot. Res. 29 (2010) 585–597.
[5] L.U. Odhner, R.R. Ma, A.M. Dollar, Open-loop precision grasping with underactuated hands inspired by a human manipulation strategy, IEEE Trans. Autom. Sci. Eng. 10 (2013) 625–633.
[6] J. Borràs, A.M. Dollar, Analyzing dexterous hands Using a Parallel Robots Framework, Auton. Robot. 36 (2014) 169–180.
[7] M.T. Mason, A. Rodriguez, S.S. Srinivasa, A.S. Vazquez, Autonomous manipulation with a general-purpose simple hand, Int. J. Robot. Res. 31 (2011) 688–703.
[8] L.U. Odhner, L. Jentoft, M.R. Claffee, N. Corson, Y. Tenzer, R. Ma, M. Buehler, R. Kohout, R.D. Howe, A.M. Dollar, A compliant, underactuated hand for robust manipulation, Int. J. Robot. Res. 33 (2014) 736–752.

[9] G.A. Kragten, F.C.T. van der Helm, J.L. Herder, A planar geometric design approach for a large grasp range in underactuated hands, Mech. Sci. 46 (2011) 1121–1136.
[10] Robert Platt, Andrew H. Fagg, Roderic A. Grupen, Null-space grasp control: Theory and experiments, IEEE Trans. Robot. 26 (2010) 282–295.
[11] S. Krut, V. Begoc, E. Dombre, F. Pierrot, Extension of the form-closure property to underactuated hands, IEEE Trans. Robot. 26 (2010) 853–866.
[12] Dalibor Petkovic, Mirna Issa, Nenad D. Pavlovic, Lena Zentner, Zarko Cojbašic, Adaptive neuro fuzzy controller for adaptive compliant robotic gripper, Expert Syst. Appl. 39 (2012) 13295–13304.
[13] Dalibor Petković, Amir Seyed Danesh, Mehdi Dadkhah, Negin Misaghian, Shahaboddin Shamshirband, Erfan Zalnezhad, Nenad D. Pavlović, Adaptive control algorithm of flexible robotic gripper by extreme learning machine, Robot. Comput.-Integr. Manuf. 37 (2016) 170–178.
[14] Rajagopalan Srinivasan, Andrzej Kraslawski, Application of the TRIZ creativity enhancement approach to the design of a passively adaptive compliant robotic gripper, Assembly Automation 33 (2013).
[15] G.P. Jung, J.S. Koh, K.J. Cho, Underactuated adaptive gripper using flexural buckling, IEEE Trans. Robot. 29 (2013) 1396–1407.
[16] M. Ciocarlie, P. Allen, A design and analysis tool for underactuated compliant hands, in: Proc. IEEE/RSJ International Conference on Intelligent Robots and Systems, October, 2009, pp. 5234–5239.
[17] M. Ciocarlie, P. Allen, A constrained optimization framework for compliant underactuated grasping, Mech. Sci. 2 (2011) 17–26.
[18] Eiman Tamah Al-Shammari, Dalibor Petković, Amir Seyed Danesh, Shahaboddin Shamshirband, Mirna Issa, Lena Zentner, Neuro-fuzzy estimation of passive robotic joint safe velocity with embedded sensors of conductive silicone rubber, Mech. Syst. Signal Process. 72–73 (2016) 486–498.
[19] M.E. Giannaccini, I. Georgilas, I. Horsfield, B.H.P.M. Peiris, A. Lenz, A.G. Pipe, S. Dogramadzi, A variable compliance, soft gripper, Auton. Robot. 36 (2014) 93–107.
[20] L. Odhner, A. Dollar, Dexterous manipulation with underactuated elastic hands, in: Proc. IEEE Int. Conf. Robot. Autom., Karlsruhe, Germany, May 2011, pp. 5254–5260.
[21] Zhongyi Chu, Jian Hu, Shan Lu, Evaluation of spring stiffness for stable grasp in underactuated fingers, Lect. Notes Electr. Eng. (2017) 57–73.
[22] Zhongyi Chu, Miao Zhou, Jian Hu, Shan Lu, Gripping mode analysis of an active-passive composited driving self-adaptive gripper mechanism, Acta Aeronaut. Astronaut. Sin. 35 (2014) 3451–3458.
[23] G.A. Kragten, M. Baril, C. Gosselin, J.L. Herder, Stable precision grasps by underactuated grippers, IEEE Trans. Robot. 27 (2011) 1056–1066.

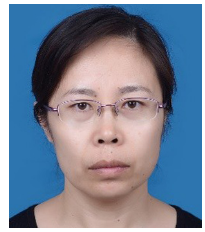

Jing Cui was born in Heilongjiang province, China, in 1976. She received the Ph.D. degree from the robotics research institute, Harbin Institute of Technology, Harbin, China, in 2004. She was a postdoctoral fellow with the department of mechanical engineering in 2007, Tsinghua University, Beijing, China. Currently, she is a associated professor with the school of mechanical engineering and applied electronics, Beijing University of Technology, Beijing, China. Her research interests include robotics and intelligent control.

Shaobo Yan is graduated student with the school of instrument science and opto-electronics, Beihang University. His research interests include robotics mechanism and intelligent control.

Jian Hu was graduated student with the school of instrument science and opto-electronics, Beihang University. His research interests include robotics mechanism and intelligent control.

ZhongYi Chu was born in Hebei province, China, in 1977. He received the Ph.D. degree from the robotics research institute, Harbin Institute of Technology, Harbin, China, in 2004. He was a postdoctoral fellow with the state key lab of intelligent technology and systems in 2006, Tsinghua University, Beijing, China. Currently, he is a professor with the school of instrument science and opto-electronics, Beihang University, Beijing, China. His research interests include robotics mechanism and intelligent control.